

NEEDATOOL: A NEEDLET ANALYSIS TOOL FOR COSMOLOGICAL DATA PROCESSING

DAVIDE PIETROBON

Jet Propulsion Laboratory, California Institute of Technology
4800 Oak Grove Dr. 91109 Pasadena CA

AMEDEO BALBI

Dipartimento di Fisica, Università di Roma “Tor Vergata”, via della Ricerca Scientifica 1, 00133 Roma, Italy
INFN Sezione di Roma “Tor Vergata”, via della Ricerca Scientifica 1, 00133 Roma, Italy

PAOLO CABELLA

Dipartimento di Fisica, Università di Roma “Tor Vergata”, via della Ricerca Scientifica 1, 00133 Roma, Italy

KRZYSZTOF M. GORSKI

Jet Propulsion Laboratory, California Institute of Technology
4800 Oak Grove Dr. 91109 Pasadena CA
Warsaw University Observatory, Aleje Ujazdowskie 4, 00478 Warszawa, Poland
Draft version October 26, 2018

Abstract

We introduce NeedATool (Needlet Analysis Tool), a software for data analysis based on needlets, a wavelet rendition which is powerful for the analysis of fields defined on a sphere. Needlets have been applied successfully to the treatment of astrophysical and cosmological observations, and in particular to the analysis of cosmic microwave background (CMB) data.

Usually, such analyses are performed in real space as well as in its dual domain, the harmonic one. Both spaces have advantages and disadvantages: for example, in pixel space it is easier to deal with partial sky coverage and experimental noise; in harmonic domain, beam treatment and comparison with theoretical predictions are more effective. During the last decade, however, wavelets have emerged as a useful tool for CMB data analysis, since they allow to combine most of the advantages of the two spaces, one of the main reasons being their sharp localisation.

In this paper, we outline the analytical properties of needlets and discuss the main features of the numerical code, which should be a valuable addition to the CMB analyst’s toolbox.

Subject headings: methods: data analysis, numerical, statistical, cosmology: observations, cosmic background radiation

Over the last two decades, the detailed analysis of cosmic microwave background radiation anisotropies has been fundamental in determining the global properties of our Universe and its evolutions. The cosmological concordance model encodes into few parameters the variety of processes we observe in the local universe as well as those occurring at very large scales. Such parameters have been measured very precisely by several CMB experiments (Mather et al. 1992; Smoot et al. 1992; de Bernardis et al. 2000; Komatsu et al. 2010). and such measurements will be further refined with the next generation of cosmological experiments. CMB data analysis is very demanding – both in terms of computational power required and sophistication of the necessary techniques – due to the complexity of the datasets and to the high degree of accuracy one wants to achieve. An overview on the techniques recently applied to astrophysical data analysis can be found in Pesenson et al. (2010). This holds in particular for cutting-edge experi-

ments such as the ongoing Planck satellite ¹.

Over the last decade, wavelets (Freeden and Schneider 1998; Antoine and Vanderghelynst 1999; McEwen et al. 2006, 2007; Sanz et al. 2006; Starck et al. 2006, 2009) have emerged as a very powerful tool for CMB data analysis; a very incomplete list of references should include testing for non-Gaussianity (Vielva et al. 2004; Cabella et al. 2004), foreground subtraction (Hansen et al. 2006), point source detection (Sanz et al. 2006), component separation (Moudden et al. 2005; Starck et al. 2006), polarisation analysis (Cabella et al. 2007) and many others. The reason for such a strong interest is easily understood. As it is well-known, CMB models are best analysed in the frequency domain, where the behaviour at different multipoles can be investigated separately; on the other hand, partial sky coverage and other missing observations make the evaluation of exact spherical harmonic transforms troublesome. The combination of these two features makes the time-frequency localisation properties of wavelets most valuable. See Starck and Bobin (2009) for a recent review on

Electronic address: davide.pietrobon@jpl.nasa.gov
Electronic address: amedeo.balbi@roma2.infn.it
Electronic address: paolo.cabella@roma2.infn.it
Electronic address: krzysztof.m.gorski@jpl.nasa.gov

¹ [http://www.rssd.esa.int/SA/PLANCK/docs/Bluebook-ESA-SCI\(2005\)1.pdf](http://www.rssd.esa.int/SA/PLANCK/docs/Bluebook-ESA-SCI(2005)1.pdf)

this topic² and Wiaux et al. (2008) and for a numerical implementation.

Recently, a novel approach to spherical wavelets has been introduced in the statistical literature by Baldi et al. (2006), adapting tools proposed in the functional analysis literature by Narcowich et al. (2006); the first application to CMB data is due to Pietrobon et al. (2006), where needlets are used to estimate (cross-)angular power spectra in order to search for dark energy imprints on the correlation between large scale structures and the CMB (Sachs and Wolfe 1967). Guilloux et al. (2007) investigate the effect of different window functions in needlets constructions; whereas Baldi et al. (2009a) provide further mathematical results on their behaviour for partially observed sky-maps. Needlets have been applied to angular power spectrum estimation in the presence of noise (Fay et al. 2008; Faÿ and Guilloux 2008), as well as to the estimation of the bispectrum (Lan and Marinucci 2008); the latter tool has been applied to the WMAP 5-year data release by Pietrobon et al. (2009) and Rudjord et al. (2009) to constrain the primordial non-Gaussianity parameter. The bispectrum formalism has been further exploited by Pietrobon et al. (2010) and Rudjord et al. (2010), who addressed the sky asymmetry issue analysing respectively the properties of 3-point correlation function, and the primordial non-Gaussianity parameter. Cabella et al. (2010) developed the bispectrum estimator including the marginalisation over the possible foreground residuals in the CMB maps, while Delabrouille et al. (2009); Ghosh et al. (2010) produced a foreground component separation algorithm. The analysis of directional data are described in Baldi et al. (2009b). Finally, the needlet formalism has been extended to the polarisation field, as discussed by Geller and Marinucci (2008); Geller and Mayeli (2008, 2009); Geller et al. (2008); Geller et al. (2009); Geller and Marinucci (2010).

The aim of this paper is to describe a numerical code, called NeedATool (Needlet Analysis Tool), which has already been used in several of the above mentioned analyses. We first provide a discussion of the needlet formalism in Sec. 1 and 2. We then describe a viable implementation of the code in Sec. 3 and we add our concluding remarks in Sec. 4.

1. NEEDLETS FRAME

Needlets enjoy several features which are not in general granted by other spherical wavelets construction. Here, we recall some of these properties and refer to Marinucci et al. (2008); Lan and Marinucci (2008) for a comprehensive mathematical discussion. Complementary mathematical analyses can be found in Geller and Mayeli (2007); Lan and Marinucci (2009); Mayeli (2008); Geller and Mayeli (2008, 2009). In particular, needlets

- do not rely on any tangent plane approximation (compare Sanz et al. 2006), and take advantage of the manifold structure of the sphere;
- being defined in harmonic space, they are computationally very convenient, and natively

adapted to standard packages such as *HEALPix*¹ (Górski et al. 2005);

- they allow for a simple reconstruction formula (see Eq. 5), where the same needlets functions appear both in the direct and the inverse transform (see also Kerkycharian et al. (2007));
- they are quasi-exponentially (i.e. faster than any polynomial) concentrated in pixel space, see Eq. 6 below;
- they are exactly localised on a finite number of multipoles; the width of this support is explicitly known, controlling the power encoded in each multipole range (see Eq. 1);
- needlets coefficients can be shown to be asymptotically uncorrelated (and hence, in the Gaussian case, independent) at any fixed angular distance, when the frequency increases.

We first recall that the spherical needlet function is defined as

$$\psi_{jk}(\hat{\gamma}) = \sqrt{\lambda_{jk}} \sum_{\ell} b\left(\frac{\ell}{B^j}\right) \sum_{m=-\ell}^{\ell} \bar{Y}_{\ell m}(\hat{\gamma}) Y_{\ell m}(\xi_{jk}); \quad (1)$$

where γ and ξ_{jk} are directions on the sphere, $Y_{\ell m}$ is a spherical harmonic function, with $\bar{Y}_{\ell m}$ identifying its complex conjugate, and $b(x)$ is a filter function defined for $x \in [1/B, B]$, which the entire needlet construction relies on. Here, we use $\{\xi_{jk}\}$ to denote a set of *cubature points* on the sphere, corresponding to frequency j ; and λ_{jk} denotes the cubature weights. In Fig. 1 the needlet profile as function of the angle between $\hat{\gamma}$ and ξ_{jk} is shown for the choice $B=2, j=8$.

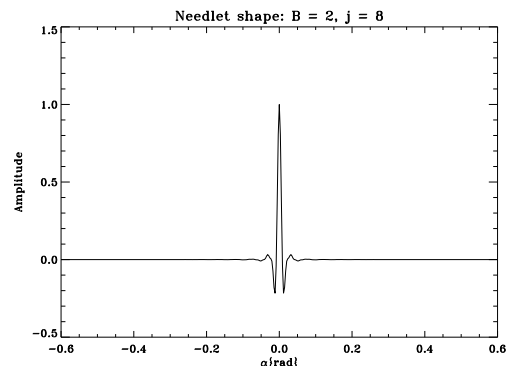


FIG. 1.— Needlets in pixel space. $B = 2, j = 8$ as a function of the angle between $\hat{\gamma}$ and ξ_{jk}

Intuitively, needlets should be viewed as a convolution of the projection operator $\sum_{m=-\ell}^{\ell} \bar{Y}_{\ell m}(\hat{\gamma}) Y_{\ell m}(\xi_{jk})$ with a suitably chosen window function $b(\cdot)$. The needlet frame construction strongly relies on the spherical harmonic decomposition which represents the mathematical environment for the derivation of the fundamental properties of needlets (Lan and Marinucci 2009): in

² A multiresolution package for data analysis and compression is also available at this url: <http://jstarck.free.fr/mresol.htm>

¹ <http://healpix.jpl.nasa.gov>

particular, the existence of a reconstruction formula, as first pointed out by Freeden and Windheuser (1997); Freeden and Schneider (1998). More details can be found in Freeden and Maier (2002). A similar approach has been followed by Starck et al. (2006, 2009), who implemented wavelets, ridgelets and curvelets built directly on the sphere, both for scalar and spin-2 fields. All these sets of functions are examples of *frames* on the sphere: they are over-complete and redundant but admit a well defined backward transformation. For this reason, frames are not only suitable for a multi-frequency analysis of a signal, as any other wavelet implementation, but also for data compression, denoising algorithm and component separation, as described by Moudden et al. (2005); Starck and Bobin (2009).

Besides spherical harmonic decomposition, needlet properties strongly depend on the filter function $b(\cdot)$, which controls the angular scale span covered by each needlet and ensures that needlets enjoy quasi-exponential localisation properties in pixel space. Formally, we must ensure that:

- i) $b^2(\cdot)$ has support in $[\frac{1}{B}, B]$, and hence $b(\frac{\ell}{B^j})$ has support in $\ell \in [B^{j-1}, B^{j+1}]$
- ii) the function $b(\cdot)$ is infinitely differentiable in $(0, \infty)$.
- iii) we have

$$\sum_{j=1}^{\infty} b^2\left(\frac{\ell}{B^j}\right) \equiv 1 \text{ for all } \ell > B. \quad (2)$$

It is immediate to see that property (i) ensures the needlets have bounded support in the harmonic domain; property (ii) is the crucial element in the derivation of the localisation properties (Narcowich et al. 2006); finally, property (iii) is necessary to establish the reconstruction formula (Eq. 5). Functions such as $b^2(\cdot)$ are called *partitions of unity*.

There are of course many possible constructions satisfying (i-iii); indeed an interesting theme of research is the derivation of optimal windows satisfying these three conditions (compare Guilloux et al. 2007), although the choice of $b(\cdot)$ is expected to exert second-order effects on the final estimates (Lan and Marinucci 2009). An explicit recipe for the construction of $b(\cdot)$ is given in Sec. 3. Very recently an extended study on how needlet properties depend on the filter functions has been conducted by Scodeller et al. (2010). Interestingly, the authors explore a peculiar construction able to mimic the Spherical Mexican Hat Wavelets based on mathematical study of Geller and Mayeli (2008, 2009).

Needlets coefficients are hence given by

$$\beta_{jk} = \sqrt{\lambda_{jk}} \sum_{\ell} b\left(\frac{\ell}{B^j}\right) \sum_{m=-\ell}^{\ell} a_{\ell m} Y_{\ell m}(\xi_{jk}). \quad (3)$$

In Fig. 2 we show the needlet coefficients of WMAP 5-year temperature map for the specific choice $B = 2$ and $j = 4$. A remarkable aspect of this construction is that the needlet coefficients can be represented easily as a Mollweide projection in the *HEALPix* pixelization framework (Górski et al. 2005), the most widely used tool for

visualization and analysis of CMB maps. This makes dealing with needlets particularly handy, since it is easy to implement a needlet analysis code which exploits pre-existing *HEALPix* routines.

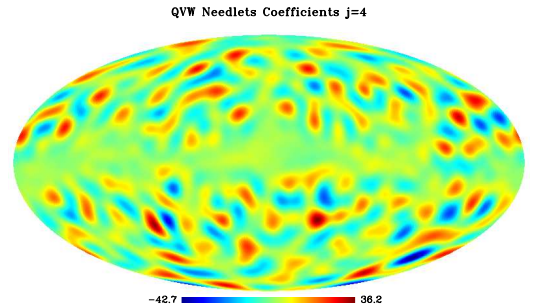


FIG. 2.— Needlet coefficients of the combined Q, V, W map at the resolution $j = 4$. The B parameter is fixed to 2. Notice as the anomalous bright spots found by Pietrobon et al. (2008) are clearly visible.

It is very important to stress that, although the needlets do *not* make up an orthonormal basis for square integrable functions on the sphere, they do represent a *tight frame*. In general, a tight frame on the sphere is a countable set of functions $\{e_j\}$ such that, for all square integrable functions on the sphere $f \in L^2(S^2)$, we have

$$\sum_j \langle f, e_j \rangle^2 \equiv \int_{S^2} f(\hat{\gamma})^2 d\Omega,$$

so that the norm is preserved. Here $\langle f, g \rangle$ means the scalar product, or more properly the projection between the functions f and g . Of course, this norm-preserving property is shared by all orthonormal systems; however, frames do not in general make up a basis, as they admit redundant elements. They can be viewed as the closest system to a basis, for a given redundancy, see Hernández and Weiss (1996), Baldi et al. (2006) and Baldi et al. (2009a) for further definitions and discussion. In our framework, the norm-preserving property translates into

$$\sum_{j,k} \beta_{jk}^2 \equiv \sum_{\ell=1}^{\infty} \frac{2\ell+1}{4\pi} \widehat{C}_{\ell}, \quad (4)$$

where

$$\widehat{C}_{\ell} = \frac{4\pi}{2\ell+1} \sum_m |a_{\ell m}|^2$$

is the angular power spectrum of the map $T(\hat{\gamma})$. Identity 4 has indeed been verified by means of numerical simulations and implicitly provides the correct normalization for needlets, λ_{jk} . It is basically a consequence of the peculiar partition-of-unity property of $b(\cdot)$ (Eq. 2). Eq. 4 is related to a much more fundamental result, i.e. the reconstruction formula

$$T(\hat{\gamma}) \equiv \sum_{j,k} \beta_{jk} \psi_{jk}(\hat{\gamma}), \quad (5)$$

which in turn is a non-trivial consequence of the analytical properties of the $b_{\ell,j}$ functions. As mentioned

before, the simple reconstruction formula of Eq. 5 is typical of tight frames but does not hold in general for other wavelets systems.

The following quasi-exponential localisation property of needlets is due to Narcowich et al. (2006) and motivates their name. For any $M = 1, 2, \dots$ there exists a positive constant c_M such that for any point $x \in S^2$ we have

$$|\psi_{jk}(\hat{\gamma})| \leq \frac{c_M B^j}{(1 + B^j \arccos(\langle x, \xi_{jk} \rangle))^M}. \quad (6)$$

We recall that $\arccos(\langle x, \xi_{jk} \rangle)$ is just the natural distance on the unit sphere between the points (x, ξ_{jk}) . The meaning of Eq. 6 is then clear: for any fixed angular distance, the value of $\psi_{jk}(\hat{\gamma})$ goes to zero quasi-exponentially in the parameter B . This clearly establish an excellent localisation behaviour in pixel space. Note that the constants c_M do depend on the form of the weight function $b(\cdot)$, and in particular on the value of the bandwidth parameter B ; typically a better localisation in multipole space (i.e., a value of B very close to unity) will entail a larger value of c_M , that is, less concentration in pixel space for any fixed j . The resulting trade-off in the behaviour over the harmonic and real spaces is expected: smaller values of B correspond to a tighter localisation in harmonic space (less multipoles entering into any needlet), whereas larger values ensure a faster decay in real space (Lan and Marinucci 2009).

In Baldi et al. (2006), another relevant property of needlets coefficients was discussed, namely their asymptotic uncorrelation at any fixed angular distance, for growing frequencies j . More explicitly, at high frequency needlets coefficients can be approximated as a sample of identically distributed and independent (under Gaussianity) coefficients. Also, in view of Eq. 3, for full sky maps and in the absence of any mask we should expect the theoretical correlation to be identically zero whenever $|j_1 - j_2| \geq 2$. This has been indeed numerically verified by Marinucci et al. (2008).

The probabilistic properties of the needlet coefficients β_{jk} have been established in Baldi et al. (2009a); in that paper, it is shown that for any two (sequence of) pixels $\xi_{jk}, \xi_{j'k'}$ such that their angular distance is larger than a positive ε , for all j , we have

$$\frac{\langle \beta_{jk} \beta_{j'k'} \rangle}{\sqrt{\langle \beta_{jk}^2 \rangle \langle \beta_{j'k'}^2 \rangle}} \leq \frac{c_M}{(s^j \varepsilon)^{M-1}} \quad \text{for all } M = 1, 2, 3, \dots \quad (7)$$

thus proving wavelets coefficients are asymptotically uncorrelated as $j \rightarrow \infty$ for any fixed angular distance. Eq. 7 can then be seen as the statistical counterpart of Eq. 6.

These properties are the basis for the large success of needlets as a CMB toolbox, in particular when dealing with masked datasets.

2. NEEDLETS ESTIMATORS: 2- AND 3- POINT CORRELATION FUNCTIONS

Having introduced the spherical needlet frame, and recalled the main properties which make needlets perform extremely well in a wide number of applications to 2-dimension fields on the sphere, we now briefly describe some important statistical techniques largely used in CMB data analysis.

2.1. (Cross-) Power Spectrum

After computing the needlets coefficients β_{jk} from a 2-dimension map (e. g. the CMB or source count map), we can use Eq. 4 to build a (cross-)correlation estimator in wavelet space, β_j , as:

$$\beta_j^{\text{IJ}} \equiv \sum_k \frac{1}{N_{\text{pix}}(j)} \beta_{jk}^{\text{I}} \beta_{jk}^{\text{J}}, \quad (8)$$

where $N_{\text{pix}}(j)$ is the number of pixels (e. g. in the *HEALPix* scheme $N_{\text{pix}} = 12N_{\text{side}}^2$) with I and J denoting the two different maps. The theoretical prediction for β_j can be computed from the expected C_ℓ^{IJ} as:

$$\beta_j^{\text{IJ}} = \sum_\ell \frac{(2\ell + 1)}{4\pi} \left[b\left(\frac{\ell}{B^j}\right) \right]^2 C_\ell^{\text{IJ}}, \quad (9)$$

where we recall $C_\ell^{\text{IJ}} \equiv \langle a_{\ell m}^{\text{I}} a_{\ell m}^{\text{J}*} \rangle$ is the (cross-) angular power spectrum.

β_j provides then an unbiased estimator for the (cross-) angular power spectrum within the needlets framework. The analytic relation between β_j and C_ℓ underlines few more advantages in using needlets. Indeed, it makes extremely easy and straightforward dealing with beam profiles and experimental window functions, which have to be taken into account when analysing real data (see Pietrobon et al. (2006)). The duality which needlets embed, namely the localisation both in pixel and harmonic domain, allows also to characterise the noise properties (see Delabrouille et al. (2009) and Pietrobon et al. (2009, 2010) for direct applications to *WMAP* 5-year data.)

Computing the 4-point correlation function, it can be easily shown that the analytical expression for the dispersion of the estimated cross-correlation power spectrum in needlet space is:

$$\Delta \beta_j^{\text{IJ}} = \sqrt{\sum_\ell \frac{(2\ell + 1)}{16\pi^2} \left[b\left(\frac{\ell}{B^j}\right) \right]^4 \left((C_\ell^{\text{IJ}})^2 + C_\ell^{\text{I}} C_\ell^{\text{J}} \right)},$$

which, of course, must be only taken as an approximation when dealing with real data, where window functions, noise and partial sky coverage have to be taken into proper account.

It is important to stress that Eq. 8 generalises into

$$\beta_{j_1 j_2}^{\text{IJ}} = \frac{1}{N_{\text{pix}}} \sum_k \beta_{j_1 k}^{\text{I}} \beta_{j_2 k}^{\text{J}}, \quad (10)$$

which describes the needlets coefficients covariance and it has been used in Pietrobon et al. (2008) to determine the degree of anomaly of a few hot and cold spots found in the CMB temperature map.

We have shown that the needlets formalism may be suitable for the problem of angular power spectrum estimation from a CMB map (and therefore, indirectly, to the estimation of cosmological parameters). In particular the application of needlets to the *WMAP* 3-year data led to interesting constraints on the dynamics of dark energy (Pietrobon et al. 2006) and to the measure of the difference in power between the two estimates of the power spectrum computed on the north and south CMB skies

(Pietrobon et al. 2008). A detailed discussion on the application of needlets to power spectrum estimation can be found in Fay et al. (2008).

2.2. Needlets Bispectrum

In the previous section we described how needlets can naturally be applied to the estimation of the 2-point correlation function and how, thanks to the reconstruction formula (Eqs. 2 and 4), it relates to the usual angular power spectrum. It is easy to extend the formalism to the higher order correlation functions.

Here, we focus on the 3-point correlation function, which plays a crucial role in CMB data analysis to detect any departure of primordial fluctuations from the Gaussian statistics, a smoking gun for non-standard inflationary models. We next briefly review the properties of the needlet bispectrum and how it relates to the spherical harmonic bispectrum. An extensive discussion is provided in Lan and Marinucci (2008); Pietrobon et al. (2009); Rudjord et al. (2009); Pietrobon et al. (2010); Rudjord et al. (2010).

The needlet bispectrum is defined as follows:

$$\begin{aligned} S_{j_1 j_2 j_3} &\equiv \frac{1}{N_{\text{pix}}} \sum_k \beta_{j_1 k} \beta_{j_2 k} \beta_{j_3 k} \\ &= \sum_{\ell_1 \ell_2 \ell_3} b_{\ell_1}^{(j_1)} b_{\ell_2}^{(j_2)} b_{\ell_3}^{(j_3)} \\ &\times \sqrt{\frac{(2\ell_1 + 1)(2\ell_2 + 1)(2\ell_3 + 1)}{4\pi}} \\ &\times \begin{pmatrix} \ell_1 & \ell_2 & \ell_3 \\ 0 & 0 & 0 \end{pmatrix} \hat{B}_{\ell_1 \ell_2 \ell_3}, \end{aligned} \quad (11)$$

where

$$\hat{B}_{\ell_1 \ell_2 \ell_3} \equiv \langle a_{\ell_1 m_1} a_{\ell_2 m_2} a_{\ell_3 m_3} \rangle = \sum_m a_{\ell_1 m_1} a_{\ell_2 m_2} a_{\ell_3 m_3}$$

is the estimated bispectrum, averaged over m 's. $S_{j_1 j_2 j_3}$ can be seen as a *binned bispectrum*, a smooth and combined component of the angular bispectrum. The bispectrum is supposed to be vanishing for a Gaussian distribution. Standard inflation mechanism (Guth 1981; Sato 1981; Linde 1982; Albrecht and Steinhardt 1982) predicts a tiny non-Gaussianity in the cosmological perturbations: this is why a great effort has been spent to measure a bispectrum amplitude different from zero in the CMB data, which would provide an extraordinary handle on the early universe physics (Smith et al. 2009; Curto et al. 2008; Komatsu et al. 2009; Natoli et al. 2010; Smidt et al. 2009; Curto et al. 2010). This kind of study is usually performed in terms of the non-linear parameter f_{NL} (see for example Komatsu and Spergel (2001); Bartolo et al. (2004); Smith and Zaldarriaga (2006)).

One of the key properties of needlets, is that the sum of the squared filter functions in harmonic space, b_{ℓ_j} , is 1 (see Eq. 2). This means that even if we group multipoles and each needlet peaks at a certain multipole range the total power is conserved. Therefore, the needlets power spectrum analysis can be in principle done with any choice of the parameter B , being the total power conserved and only the correlation and localisation properties affected by different width of b_{ℓ_j} . We incidentally

notice that any wavelet function defined as the difference between the square roots of the scaling functions at two different resolutions satisfies Eq. 2, but the uncorrelation properties are in general not granted, since they are determined by the shape of the filter function $b_{\ell}(\cdot)$. See for example Scodeller et al. (2010) for a detailed discussion on needlet filters.

This does not hold any more when the the cubic power of the filter functions contributes to the estimator used, which is indeed the case of the skewness expression and more generally of the bispectrum one. This fact is displayed in Fig. 3 where we plot the sum of square and cube of the filters functions. The not uniform sampling of the multipoles for a n-power estimator suggests that the choice of the B parameter is crucial for the analysis and must be driven by the insight on the range of multipoles to be probed.

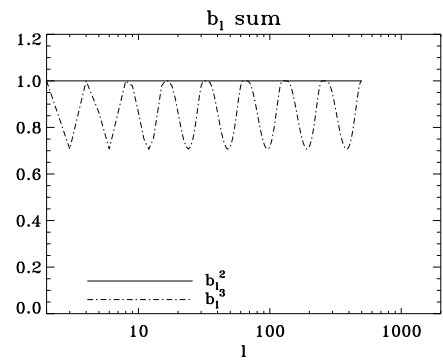


FIG. 3.— Solid line sum of the b_{ℓ}^2 ; dot-dashed line sum of the b_{ℓ}^3 . While the former is equal to 1 for the entire range of multipole, the latter is not.

3. NEEDATOOL: A NUMERICAL IMPLEMENTATION OF NEEDLETS

In the previous sections we have discussed the main needlet properties, which are indeed strictly related to the analytical properties of the filter function in harmonic space, $b(\ell/B^j)$. We now give a specific recipe for the construction of $b(\cdot)$, and describe the main features of “NeedATool” Needlet Analysis Tool - a numerical code which computes the filter functions and the needlet coefficients according to the algorithm which has been applied in the several cosmological analyses (Pietrobon et al. 2006, 2008, 2009, 2010; Cabella et al. 2010).

We give a step-by-step procedure, as implemented in NeedATool and described in Marinucci et al. (2008).

1. Construct the function

$$f(t) = \begin{cases} \exp(-\frac{1}{1-t^2}), & -1 \leq t \leq 1 \\ 0, & \text{otherwise} \end{cases}.$$

It is immediate to check that the function $f(\cdot)$ is C^∞ and compactly supported in the interval $(-1, 1)$;

2. Construct the function

$$\psi(u) = \frac{\int_{-1}^u f(t) dt}{\int_{-1}^1 f(t) dt}.$$

The function $\psi(\cdot)$ is again C^∞ ; it is moreover non-decreasing and normalised so that $\psi(-1) = 0$, $\psi(1) = 1$;

3. Construct the function

$$\varphi(t) = \begin{cases} 1 & \text{if } 0 \leq t \leq \frac{1}{B} \\ \psi(1 - \frac{2B}{B-1}(t - \frac{1}{B})) & \text{if } \frac{1}{B} \leq t \leq 1 \\ 0 & \text{if } t > 1 \end{cases}$$

Here we are simply implementing a change of variable so that the resulting function $\varphi(\cdot)$ is constant on $(0, B^{-1})$ and monotonically decreasing to zero in the interval $(B^{-1}, 1)$. Indeed it can be checked that

$$1 - \frac{2B}{B-1}(t - \frac{1}{B}) = \begin{cases} 1 & \text{for } t = \frac{1}{B} \\ -1 & \text{for } t = 1 \end{cases}$$

and

$$\begin{aligned} \varphi(\frac{1}{B}) &= \psi(1) = 1 \\ \varphi(1) &= \psi(-1) = 0; \end{aligned}$$

4. Construct

$$b^2(\xi) = \varphi(\frac{\xi}{B}) - \varphi(\xi)$$

The expression for $b^2(\cdot)$ is meant to ensure that the function satisfies the partition-of-unity property of Eq. 2. Needless to say, for $b(\xi) = \{\varphi(\frac{\xi}{B}) - \varphi(\xi)\}^{1/2}$ we take the positive root.

Incidentally, we notice that property 4 is crucial in allowing for the reconstruction formula, and it is shared, although within a different setup, by the implementation described by Starck et al. (2006, 2009) who makes use of the *HEALPix* software package too. In Fig. 4 we show the set of filter functions in ℓ space for the choice $B = 2$. They result in a homogeneous binning in $\log \ell$, whose power sum to 1, a crucial property which needlets properties rely on.

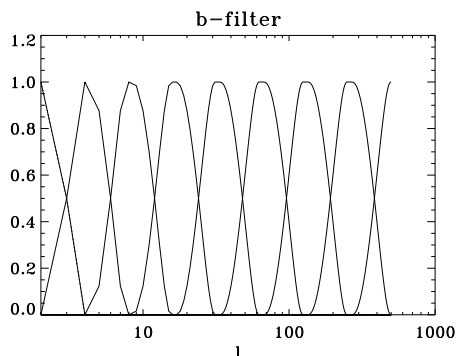


FIG. 4.— Filter function in ℓ -space which the needlet construction relies on. Set computed for $B = 2$.

NeedATool² computes the needlet filter functions in harmonic space and the needlets coefficients, given a

² http://www.fisica.uniroma2.it/~pietrobon/dp_webpage_eng.html

set of parameters. The code is based on the public available *HEALPix* package³ (Górski et al. 2005), which has to be downloaded and installed separately (version 2.10 or higher required). The software is composed of two programs “*synneed*” and “*ananeed*”; following the *HEALPix* structure the former deconvolves a given map to obtain a needlet frame, the latter reconstructs the original map, if a needlets basis is given as input. Both the programs, as well as the routines necessary for NeedA-Tool will be fully integrated in the next *HEALPix* release. Both the programs accept the same parsing file in which the fundamental parameters are provided by the user. A list of such parameters is given in Tab. 1. The maximum number of multipoles (ℓ_{\max}) and the B parameter are required. Those given, the codes computes the maximum j necessary to keep all the information in the map. The N_{side} of the needlets coefficients is then determined according to the relation $\ell_{\max} \leq 2N_{\text{side}}$. The filter functions $b_{\ell j}$ are computed by default, while it is possible to choose whether computing the needlet coefficients, which actually is the most time-consuming part, by setting the keyword “*compute_needlets*”. It is necessary then to specify the map and its resolution. A sky mask can be applied filling the “*maskfile*” variable. The last two keywords set the output files. The input map of *ananeed* has to be the needlet output file created by *synneed*.

The cubature points $\mathcal{X}_j = \{\xi_{jk}\}_{k=1,2,\dots}$, are assumed to coincide with the pixelization of the unit sphere \mathbb{S}^2 provided by *HEALPix*, with N_{side} such that $\ell_{\max} \equiv [B^{j+1}] \leq 2N_{\text{side}}$ (with $[\cdot]$ denoting the integer part and $B > 1$). The cubature weights, λ_{jk} are given by $1/N_{\text{pix}}$, with N_{pix} given by $12 \cdot N_{\text{side}}^2$. We then computed the β_{jk} coefficients for each k position given by the *HEALPix* scheme evaluating the projection operator, namely the product of $\sum_{\ell\ell'} Y_{\ell m} \bar{Y}_{\ell' m'}$ for each pair of pixels ξ_{jk} , by means of the *HEALPix* software package. The code is very fast, and it can be run on a laptop. For a low resolution map ($N_{\text{side}} = 256$), it takes a few seconds, while it scales according the *HEALPix* scaling laws for higher resolutions.

We present an example of the reconstruction power of the needlet frame. We produced a CMB map consistent with the WMAP 5-year best fit cosmological power spectrum (Komatsu et al. 2009) up to $\ell_{\max} = 500$ by using the *HEALPix* toolbox.

We processed this map through the needlet pipeline extracting first the needlet coefficients by applying *synneed*, then reconstructing the map using *ananeed*. We repeated this procedure both for the whole sky case and in presence of symmetric sky cuts, 15° , 5° , 1° and 0.1° . The results are shown in Fig. 5 (left column) together with the percentage error due to the procedure (right column). The error due to the forward and backward transformation is smaller than 0.01% except for few pixels in the whole sky case. The result worsens reaching 1% when a broad mask is applied, basically because the needlet coefficients at very large scale are affected by the presence of the mask. This effect is actually expected, since needlets work well at small angular scales, namely when the filter function $b(\ell/B^j)$ groups several multi-

³ <http://healpix.jpl.nasa.gov/>

TABLE 1
PARAMETERS REQUIRED BY THE CODES “SYNNEED” AND “ANANEED”.

Parameter	synneed	Ananeed
healpix_dir	/usr/local/Healpix.2.13a	
ℓ_{\max}	500	
B	2.0	
compute_needlets	T	
mapfile	input/lcdm_map_lmax500.fits	needlet_2.00_Nj009.fits
mapside	256	256
maskfile	input/sky_cut_1_256_ring.fits	input/sky_cut_1_256_ring.fits
bl2_root	bl2	
need_root	needlet	recmap

poles. The mask effect may be reduced by either fine tuning the B parameter, or deconvolving the mask effect. Reconstruction error is indeed wavelet frame dependent: a better performance can be achieved when the wavelet is defined as the difference between two scaling functions at two different resolutions instead of the difference between the square root of the scaling functions. This is the implementation discussed by Starck et al. (2006) which leads to an exact reconstruction.

To give another estimate of the error due to the reconstruction, we computed the angular power spectrum of the original map, C_ℓ , as well those of the reprocessed ones, C_ℓ^R , and compared them. The ratio is displayed in Fig. 6 (left panel) for the four analysed sky cuts applied. The full sky reconstruction shows an excellent agreement, the difference between the power spectra being of the order of 10^{-4} ; when a mask is present, the reconstruction causes an error of few percent at very low angular scales, which decreases at small scales.

The non perfect reconstruction in presence of missing information is expected. Therefore, it is interesting to compare the needlets performance to the one of the spherical harmonics implemented by *HEALPix*. We extracted the $a_{\ell m}$ from the same CMB realisation for the five different sky coverages considered by using *anafast*; then we produced a CMB map out of the *pseudo- $a_{\ell m}$* using *synfast*. We finally analysed the resulting map computing its power spectrum. The difference with respect the power spectrum computed through needlets is shown in the right panel of Fig. 6. The spectra agree very well regardless the applied mask. This confirms the high performance of needlets in reconstructing a field in the sphere. As a further figure of merit, we show in Fig. 7 the percentage error between the two maps reconstructed using spherical harmonics and needlets for the broadest mask (15°). The agreement is striking: a large scale pattern appears at the level of $< 1\%$.

We further investigate the mask effect, focusing on how the presence of a sky cut couples the spherical harmonics coefficients. As it is well known, in the case of partial sky coverage the spherical harmonics do not form an orthonormal basis. This can be formalized as follows:

$$T^R(\hat{\gamma}) = \sum_{\ell m} \tilde{a}_{\ell m} Y_{\ell m}(\hat{\gamma}) \quad (12)$$

$$\tilde{a}_{\ell' m'} = \int_{\mathcal{O}} T(\hat{\gamma}) \bar{Y}_{\ell' m'} d\Omega = \sum_{\ell m} a_{\ell m} \mathcal{K}_{\ell \ell' m m'} \quad (13)$$

$$\int_{\Omega} \bar{Y}_{\ell' m'}(\hat{\gamma}) Y_{\ell m}(\hat{\gamma}) W(\hat{\gamma}) d\Omega \equiv \mathcal{K}_{\ell \ell' m m'}, \quad (14)$$

where \mathcal{O} is the observed region and $\mathcal{K}_{\ell \ell' m m'}$ is the coupling matrix. In the needlet framework, this affects the

β_{jk} coefficients as:

$$\tilde{\beta}_{jk} = \sqrt{\lambda_{jk}} \sum_{\ell' m'} b\left(\frac{\ell'}{B^j}\right) \tilde{a}_{\ell' m'} Y_{\ell' m'}(\xi_{jk}) \quad (15)$$

$$T^R(\hat{\gamma}) = \sum_j \sum_{\ell' m'} b\left(\frac{\ell'}{B^j}\right) \tilde{a}_{\ell' m'} \sum_{\ell m} b\left(\frac{\ell}{B^j}\right) Y_{\ell m}(\hat{\gamma}) \mathcal{K}_{\ell \ell' m m'}. \quad (16)$$

As for the spherical harmonics decomposition, the map reconstructed through the needlet pipeline is computed from $\tilde{a}_{\ell m}$; in addition, the mask shows indirectly its effect on the filter functions $b(\ell/B^j)$.

To visualize this effect, we plot in Fig. 8 the coupling matrix $\mathcal{K}_{\ell \ell' m m'}$ for a full sky case (upper panel), in which it actually becomes a Kronecker’s δ function, $\delta_{\ell \ell' m m'}$; for a 15° symmetric sky cut (middle panel) and for the convolution $\sum_j b(\ell'/B^j) \mathcal{K}_{\ell \ell' m m'} b(\ell/B^j)$, which appears in Eq. 16. Since the numerical evaluation of the coupling matrix up to $\ell = 500$ is a severe computational challenge and we expect the higher multipoles to be marginally affected by a partial sky coverage, we computed Eq. 14 on a smaller range of spherical harmonics in the interval $\ell \in [0, 20]$ on the *HEALPix* pixelization at $N_{\text{side}} = 16$. The presence of the mask translates into off-diagonal terms in Fig. 8: each multipole is coupled to its second neighbor, whereas the coupling with the first neighbor is vanishing because of parity. The coupling is indeed not negligible up to the fourth second neighbor. The lower panel in Fig. 8 clearly depicts the properties of needlets and explain the error we obtain in the reconstruction. The correlation matrix results a superposition of blocks, each of them corresponding to a given j : each block partially overlaps only the first neighbor, as a consequence of the compact support of the $b(\ell/B^j)$ functions. (This is shown by the white regions we observe in the plot). Moreover, the off-diagonal elements are less powerful compared to the auto-correlation terms and the correlation extends to a lower number of multipoles. At very large scale however, a lack of power is present in the diagonal terms which affects the global reconstructed map. This can be seen in the right panel of Fig. 5, where the error in the reconstructed map follows a peculiar pattern which results symmetric as a consequence of the sky cut.

The additional coupling due to the mask present in the needlet construction arises from the definition of needlet itself, Eq. 1, since the needlet is built from the projection operator. However, needlets provide a natural way to counterbalance this effect. At large scale, the needlets are not sharply localised, and the coefficients turn out to be non-vanishing also in the masked region. Taking into

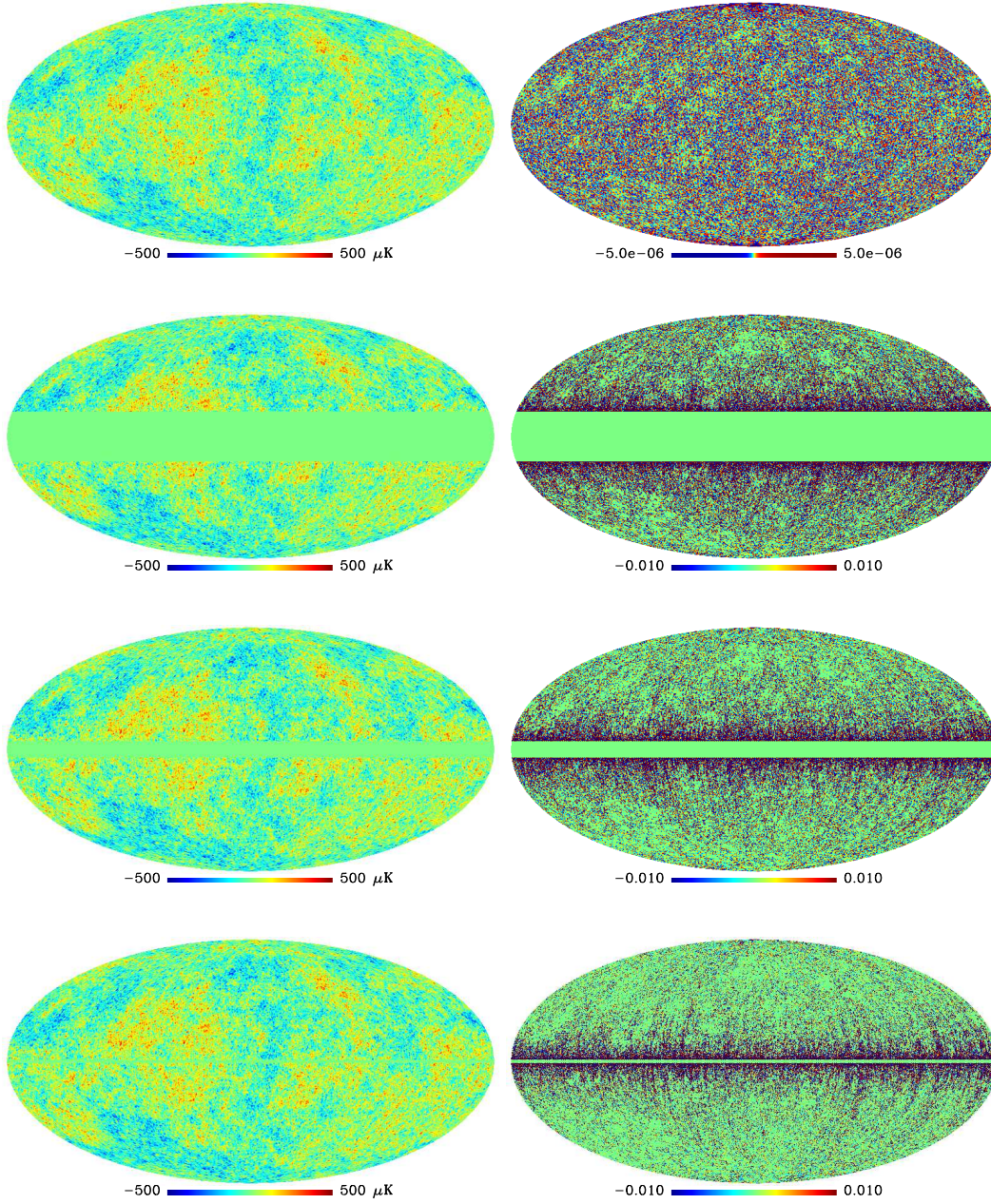


FIG. 5.— Left: reconstructed maps for the several sky cuts analysed (from top to bottom full-sky, 15° , 5° and 1°); right: percentage error on the reconstructed map.

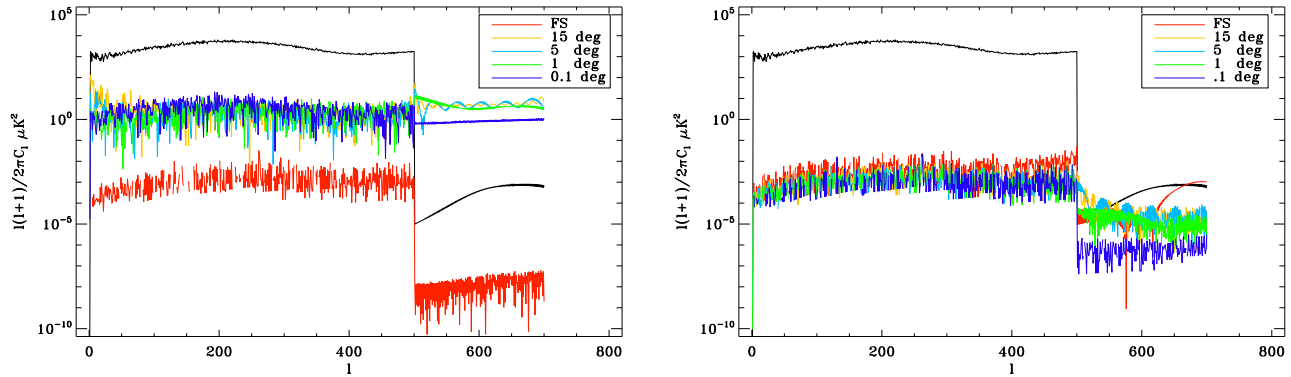


FIG. 6.— Left panel: absolute value of the difference between the power spectra extracted from the original map and the reconstructed one for several symmetric sky cuts: full sky (red solid line), 15° (yellow solid line), 5° (light blue solid line), 1° (green solid line) and 0.1° (blue solid line). The black solid line shows the CMB angular power spectrum for the original map. Right panel: comparison between the reconstruction using *synfast-anafast* combination and the needlets pipeline for the same sky cuts. The input angular power spectrum contains information up to $\ell = 500$, but we computed the power spectrum of the realization map up to $\ell = 700$ to check the leakage from low multipoles to high ones: this explains the edge at $\ell = 500$ in the plotted power spectra.

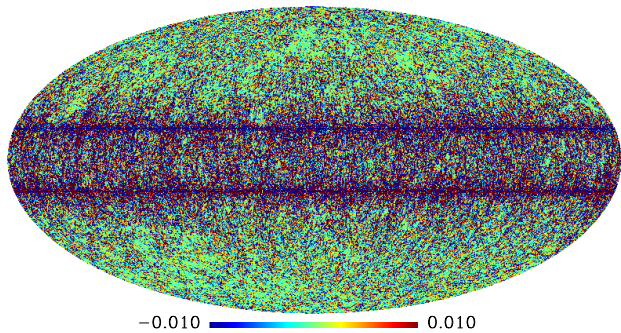


FIG. 7.— Percentage error between the two maps reconstructed using spherical harmonics and needlets. A symmetric sky cut of 15° is applied. The agreement is impressive.

account this leakage, and including in the reconstruction procedure the coefficients inside the mask, it is possible to reduce the effect of the coupling between needlets. This is the actual procedure implemented in the code, which leads to the results discussed in this section. The residual effect due to the presence of the mask shows up in the large scale pattern highlighted in Fig. 7.

4. CONCLUSIONS

In this paper we have introduced NeedATool, a public software for the analysis of datasets on the sphere based on the needlet framework. The software is particularly useful for the analysis of CMB data, as shown by its successful application to, e.g., the WMAP dataset. The needlet construction differs from other wavelet renditions due to the distinctive properties of the filter functions $b_{\ell j}$, which translate into a sharp localisation in pixel space and excellent properties of non-correlation among the functions of the set. This aspect is crucial when building estimators for CMB data analysis as we discussed extensively: therefore, needlets are a very promising tool for high-accuracy cosmological experiments.

ACKNOWLEDGEMENTS

We thank Domenico Marinucci for useful discussions and Giancarlo de Gasperis and Rajib Saha for technical support.

REFERENCES

- J. C. Mather et al., in *American Institute of Physics Conference Series*, edited by H. J. Haubold and R. K. Khanna (1992), vol. 245 of *American Institute of Physics Conference Series*, pp. 266–278.
- G. F. Smoot et al., *ApJ* **396**, L1 (1992).
- P. de Bernardis et al. (Boomerang), *Nature* **404**, 955 (2000), astro-ph/0004404.
- E. Komatsu, K. M. Smith, J. Dunkley, C. L. Bennett, B. Gold, G. Hinshaw, N. Jarosik, D. Larson, M. R.olta, L. Page, et al., *ArXiv e-prints* (2010), 1001.4538.
- M. Z. Pesenson, I. Z. Pesenson, and B. McCollum, *Advances in Astronomy* **2010** (2010), 1003.0879.
- W. Freedman and F. Schneider, *Inverse Problems* **14**, 225 (1998).
- J.-P. Antoine and P. Vandergheynst, *Appl. Comput. Harmon. Anal.* **7**, 262 (1999), ISSN 1063-5203.
- J. D. McEwen, M. P. Hobson, and A. N. Lasenby, *arXiv: 0609159* (astro-ph) (2006), astro-ph/0609159.
- J. D. McEwen, P. Vielva, M. P. Hobson, E. Martínez-González, and A. N. Lasenby, *MNRAS* **376**, 1211 (2007), arXiv:astro-ph/0602398.
- J. L. Sanz, D. Herranz, M. Lopez-Caniego, and F. Argueso, *Proceedings of the 14th European Signal Processing Conference (EUSIPCO 2006)*, Florence (Italy), September 4-8 2006, Eds. F. Gini and E.E. Kuruoglu (2006), astro-ph/0609351.
- J.-L. Starck, Y. Moudren, P. Abrial, and M. Nguyen, *A&A* **446**, 1191 (2006), arXiv:astro-ph/0509883.
- J. Starck, Y. Moudren, and J. Bobin, *A&A* **497**, 931 (2009), 0902.0574.
- P. Vielva, E. Martínez-González, R. B. Barreiro, J. L. Sanz, and L. Cayón, *ApJ* **609**, 22 (2004), arXiv:astro-ph/0310273.
- P. Cabella, F. Hansen, D. Marinucci, D. Pagano, and N. Vittorio, *Phys. Rev. D* **69**, 063007 (2004), arXiv:astro-ph/0401307.
- F. K. Hansen, A. J. Banday, H. K. Eriksen, K. M. Górski, and P. B. Lilje, *ApJ* **648**, 784 (2006), arXiv:astro-ph/0603308.

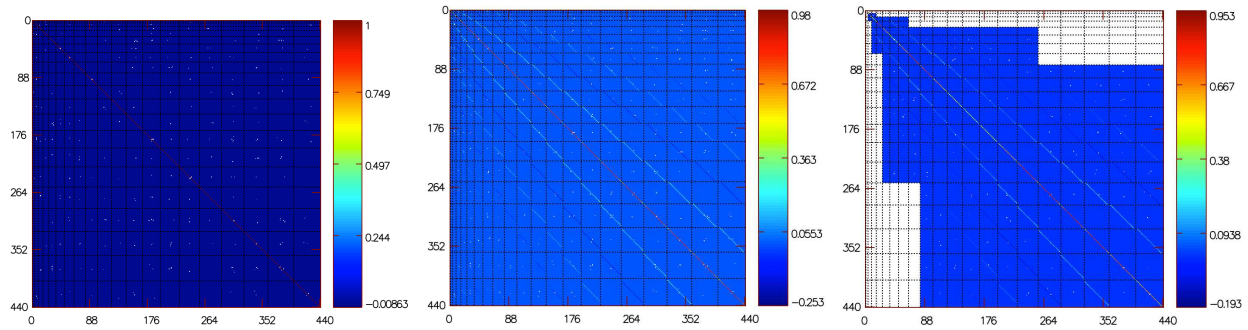


FIG. 8.— Coupling matrix as a function of the quantity $\ell^2 + \ell + m + 1$ for three interesting cases: full sky (left panel), 15° symmetric sky cut (middle panel) and its convolution with needlet window functions (right panel). The grid marks the multipoles.

- Y. Moudden, J. F. Cardoso, J. L. Starck, and J. Delabrouille, *EURASIP J. Appl. Signal Process.* **15**, 2437 (2005), astro-ph/0407053.
- P. Cabella, P. Natoli, and J. Silk, *Phys. Rev. D* **76**, 123014 (2007), arXiv:0705.0810.
- J. Starck and J. Bobin, *ArXiv e-prints* (2009), 0903.3383.
- Y. Wiaux, J. D. McEwen, P. Vanderghyest, and O. Blanc, *MNRAS* **388**, 770 (2008), 0712.3519.
- P. Baldi, G. Kerkycharian, D. Marinucci, and D. Picard, *Annals of Statistics* 2009, No. 3, 1150-1171 **37**, 1150 (2006), arXiv:math/0606599.
- F. J. Narcowich, P. Petrushev, and J. D. Ward, *SIAM J. Math. Anal.* **38**, 574 (2006), ISSN 0036-1410.
- D. Pietrobon, A. Balbi, and D. Marinucci, *Phys. Rev. D* **74**, 043524 (2006), arXiv:astro-ph/0606475.
- R. K. Sachs and A. M. Wolfe, *ApJ* **147**, 73 (1967).
- F. Guilloux, G. Fay, and J.-F. Cardoso, arXiv: 0706.2598 (math NA) (2007), 0706.2598.
- P. Baldi, G. Kerkycharian, D. Marinucci, and D. Picard, *Bernoulli* **15**, 438 (2009a), 0706.4169.
- G. Fay et al., *Phys. Rev. D* **78**, 083013 (2008), 0807.1113.
- G. Faÿ and F. Guilloux, arXiv: 0807.2162 (2008), arXiv: 0807.2162.
- X. Lan and D. Marinucci, *Elec. Jour. of Stats.* 2008, Vol. 2, 332-367 **802** (2008).
- D. Pietrobon, P. Cabella, A. Balbi, G. de Gasperis, and N. Vittorio, *MNRAS* **396**, 1682 (2009), 0812.2478.
- Ø. Rudjord, F. K. Hansen, X. Lan, M. Liguori, D. Marinucci, and S. Matarrese, *ApJ* **701**, 369 (2009), 0901.3154.
- D. Pietrobon, P. Cabella, A. Balbi, R. Crittenden, G. de Gasperis, and N. Vittorio, *MNRAS* **402**, L34 (2010), 0905.3702.
- Ø. Rudjord, F. K. Hansen, X. Lan, M. Liguori, D. Marinucci, and S. Matarrese, *ApJ* **708**, 1321 (2010), 0906.3232.
- P. Cabella, D. Pietrobon, M. Veneziani, A. Balbi, R. Crittenden, G. de Gasperis, C. Quercellini, and N. Vittorio, *MNRAS* **405**, 961 (2010), 0910.4362.
- J. Delabrouille, J.-F. Cardoso, M. Le Jeune, M. Betoule, G. Fay, and F. Guilloux, *A&A* **493**, 835 (2009), 0807.0773.
- T. Ghosh, J. Delabrouille, M. Remazeilles, J. Cardoso, and T. Souradeep, *ArXiv e-prints* (2010), 1006.0916.
- P. Baldi, G. Kerkycharian, D. Marinucci, and D. Picard, *Annals of Statistics* **37**, 3362 (2009b), 0807.5059.
- D. Geller and D. Marinucci, *Journal of Fourier Analysis and Applications*, online first (2010) (2008), 0811.2935.
- D. Geller and A. Mayeli, *ArXiv e-prints* (2008), 0811.4440.
- D. Geller and A. Mayeli, *ArXiv e-prints* (2009), 0907.3164.
- D. Geller, F. K. Hansen, D. Marinucci, G. Kerkycharian, and D. Picard, *Phys. Rev. D* **78**, 123533 (2008), 0811.2881.
- D. Geller, X. Lan, and D. Marinucci, *Electronic Journal of Statistics* **3**, 1497 (2009), 0907.3369.
- D. Geller and D. Marinucci, *ArXiv e-prints* (2010), 1006.3835.
- D. Marinucci, D. Pietrobon, A. Balbi, P. Baldi, P. Cabella, G. Kerkycharian, P. Natoli, D. Picard, and N. Vittorio, *MNRAS* **383**, 539 (2008), arXiv:0707.0844.
- D. Geller and A. Mayeli, *Nearly tight frames and space-frequency analysis on compact manifolds* (2007), arXiv: 0706.3642.
- X. Lan and D. Marinucci, *Stochastic Processes and their Applications* **119**, 3749 (2009), 0805.4154.
- A. Mayeli, *Asymptotic uncorrelation for mexican needlets* (2008), arXiv: 0806.3009.
- K. M. Górski, E. Hivon, A. J. Banday, B. D. Wandelt, F. K. Hansen, M. Reinecke, and M. Bartelmann, *ApJ* **622**, 759 (2005), arXiv:astro-ph/0409513.
- G. Kerkycharian, P. Petrushev, D. Picard, and T. Willer, *Elec. Jour. of Stats.* **1**, 30 (2007).
- W. Freeden and U. Windheuser, *Applied and Computational Harmonic Analysis* **4**, 1 (1997).
- W. Freeden and T. Maier, *Electronic Transactions on Numerical Analysis (ETNA)* **14**, 40 (2002).
- S. Scodeller, O. Rudjord, F. K. Hansen, D. Marinucci, D. Geller, and A. Mayeli, *ArXiv e-prints* (2010), 1004.5576.
- D. Pietrobon, A. Amblard, A. Balbi, P. Cabella, A. Cooray, and D. Marinucci, *Phys. Rev. D* **78**, 103504 (2008), 0809.0010.
- E. Hernández and G. Weiss, *A first course on wavelets*, Studies in Advanced Mathematics (CRC Press, Boca Raton, FL, 1996), ISBN 0-8493-8274-2, with a foreword by Yves Meyer.
- A. H. Guth, *Phys. Rev. D* **23**, 347 (1981).
- K. Sato, *MNRAS* **195**, 467 (1981).
- A. D. Linde, *Phys. Lett. B* **108**, 389 (1982).
- A. Albrecht and P. J. Steinhardt, *Phys. Rev. Lett.* **48**, 1220 (1982).
- K. M. Smith, L. Senatore, and M. Zaldarriaga, *JCAP* **9**, 6 (2009), 0901.2572.
- A. Curto, J. F. Macías-Pérez, E. Martínez-González, R. B. Barreiro, D. Santos, F. K. Hansen, M. Liguori, and S. Matarrese, *A&A* **486**, 383 (2008), 0804.0136.
- E. Komatsu et al. (WMAP), *ApJ* **180**, 330 (2009), 0803.0547.
- P. Natoli, G. de Troia, C. Hikage, E. Komatsu, M. Migliaccio, P. A. R. Ade, J. J. Bock, J. R. Bond, J. Borrill, A. Boscaleri, et al., *MNRAS* pp. 1266+ (2010), 0905.4301.
- J. Smidt, A. Amblard, P. Serra, and A. Cooray, *Phys. Rev. D* **80**, 123005 (2009), 0907.4051.
- A. Curto, E. Martinez-Gonzalez, and R. B. Barreiro, *ArXiv e-prints* (2010), 1007.2181.
- E. Komatsu and D. N. Spergel, *Phys. Rev. D* **63**, 063002 (2001), arXiv:astro-ph/0005036.
- N. Bartolo, E. Komatsu, S. Matarrese, and A. Riotto, *Phys. Rep.* **402**, 103 (2004), arXiv:astro-ph/0406398.
- K. M. Smith and M. Zaldarriaga, arXiv: 0612571 (astro-ph CO) (2006), arXiv:astro-ph/0612571.